Corrosion Protection of Steel and Bond Durability at Polyphenylene Sulfide-to-Anhydrous Zinc Phosphate Interfaces

T. SUGAMA* and N. R. CARCIELLO

Energy Efficiency and Conservation Division, Department of Applied Science,
Brookhaven National Laboratory, Upton, New York 11973

SYNOPSIS

To enhance the performance of high-temperature polyphenylene sulfide (PPS) coating in protecting steels from corrosion, the cold-rolled steel surfaces were prepared with anhydrous zinc phosphate (Zn · Ph) conversion coatings containing poly(acid)anhydride as an interfacial tailoring material. The factors contributing to the formation of a good bond at the PPS/Zn · Ph joints were as follows: (1) the chemical reaction of PPS with Fe_2O_3 in the Zn · Ph layers, (2) PPS-to-poly(acid)anhydride interaction, and (3) the mechanical interlocking between PPS and the rough Zn · Ph crystal surfaces. Although such interfacial bond structures provide a superior durability of PPS/Zn · Ph joints against a hot H_2SO_4 solution, the cathodic reaction, $H_2O + \frac{1}{2}O_2 + 2e^- = 2OH^-$, occurring at any defect in the PPS/Zn · Ph joint system when NaCl is present will lead to the delamination of the PPS film from the phosphated steel. This cathodic delamination was due mainly to alkali-induced dissolution of Zn · Ph layers. However, the rate of delamination for the PPS/Zn · Ph systems was considerably lower compared with that for the PPS/steel system in the absence of Zn · Ph.

INTRODUCTION

In our recent studies on the interfacial bonding between polyphenylene sulfide (PPS) coatings and metal substrates, such as cold-rolled, stainless, and galvanized steels, we found that the degree of bond strength of PPS-to-metal joints depended primarily on the species of sulfur-related interfacial reaction products generated by the gas–solid chemical reaction between the metal oxides present at the outermost surface site of substrates and the SO_2 and SO_3 gases emitted from PPS at a high temperature of 350°C.[1] The order of these reaction compounds, which play an important role in developing bond strength, was $Fe_2(SO_4)_3 > FeSO_4 > FeS$. However, although such S-related iron reaction compounds significantly improved bond strength, it is well known[2-4] that these compounds commonly act to promote the corrosion rate of steels. To avoid the direct contact of PPS with steel, we also investigated the effectiveness of zinc phosphate (Zn · Ph) conversion coatings, deposited on the steel surfaces, in decreasing the cathodic delamination rate of PPS film from the zinc-phosphated steels.[5] The cathodic reaction, in terms of the oxygen reduction reaction occurring at the corrosion sites of steel in a near-neutral aqueous environment, is $H_2O + \frac{1}{2}O_2 + 2e^- = 2OH^-$. The large number of hydroxyl ions generated by this cathodic reaction creates a high pH environment underneath the PPS layers. The attack of alkali solution on the crystalline Zn · Ph coating layer frequently causes its dissolution, thereby resulting in a high rate of delamination of the PPS film. Our previous investigation suggested that the anhydrous α-$Zn_3(PO_4)$ phase derived from thermal dehydration of the original Zn · Ph hydrate phase has a low susceptibility to alkali-catalyzed dissolution.[6]

* To whom correspondence should be addressed.

Journal of Applied Polymer Science, Vol. 45, 1291–1301 (1992)
 CCC 0021-8995/92/071291-11$04.00

Accordingly, the emphasis of this article was directed toward obtaining a better understanding and visualization of the chemical changes at the PPS-to-α phase interfacial contact zones, which are important in improving the durability of adhesive bond and reducing the rate of cathodic delamination of PPS film. For comparison, the interface of PPS-to-cold-rolled steel was also explored.

EXPERIMENTAL

Materials

The metal substrate used was AISI 1010 cold-rolled steel containing 0.08–0.13 wt % C, 0.3–0.6 wt % Mn, 0.04 wt % P, and 0.05 wt % S. The formulation of the zinc phosphate liquid was 1.3 wt % zinc orthophosphate dihydrate [$Zn_3(PO_4)_2 \cdot 2H_2O$], 2.6 wt % H_3PO_4, 2.0 wt % [25% poly(acrylic)acid, p(AA)], 1.0 wt % $Ni(NO_3)_2 \cdot 6H_2O$, and 93.1 wt % water. The average molecular weight of p(AA) polyelectrolyte, supplied by Rohm and Hass Company, was $\approx$ 60,000.

In preparing the zinc phosphate (Zn · Ph) samples, the steel surfaces were wiped with acetone-soaked tissues to remove any surface contamination from mill oil. The steel then was immersed for up to 20 min in the Zn · Ph conversion solutions at a temperature of 80°C. Finally, the deposited Zn · Ph layers were baked in an oven at 350°C for 2 h to prepare the anhydrous Zn · Ph layers.

PPS powder for the slurry coating was supplied by the Phillips 66 Company. The as-received PPS was a finely divided, tan powder having a high melt flow with a melting point of 288°C. The PPS film was deposited on the surfaces of the cold-rolled steel and Zn · Ph-treated steel substrate in the following way. First, the substrates were dipped into a PPS slurry consisting of 45 wt % PPS and 55 wt % isopropylalcohol at 25°C. Then, the slurry-coated substrates were preheated in the air at 300°C for 3 h to trigger the fusion of the PPS powder and, at the same time, the volatilization of the isopropylalcohol liquid phase. To assemble the crosslinked and extended macromolecular structures, the fused PPS was finally heated in air at 350°C for 2 h.

Measurements

The chemical compositions and states present on a bond-failure site at the interfaces of PPS/substrate joint systems were explored using X-ray photoelectron spectroscopy (XPS), scanning electron microscopy (SEM), and energy-dispersion X-ray spectrometry (EDX). The XPS used was a V.G. Scientific ESCA 3MK II. The excitation radiation was provided by an Al Kα (1486.6 eV) X-ray source, operated at a constant power of 200 W. The vacuum in the analyzer chamber of the instrument was maintained at 10^{-9} Torr. The atomic concentrations and ratios for the respective chemical elements were determined by comparing the XPS peak areas, which were obtained from the differential cross-sections for core-level excitation. To set a scale in all the high-resolution XPS spectra, the binding peak was fixed at 285.0 eV as an internal reference. A curve-deconvolution technique was employed to find the individual chemical states from the high-resolution spectra of each element. All measurements were made at an electron take-off angle of 38°, which corresponds to an analysis depth of $\approx$ 5 nm.[7] EDX is extremely useful for the quantitative analysis of any elements that exist on a surface solid layer up to $\approx$ 2 μm in thickness.

The cathodic delamination tests for the PPS-coated anhydrous Zn · Ph specimens were conducted in an air-covered 1.0 M NaCl solution using an applied potential of −1.5 V vs. SCE for up to 8 days (see Fig. 1). Thickness of Zn · Ph layer deposited on the steel substrates with the 100 × 100 mm square area was determined to be approximately 30 μm using a surface profile measuring system. PPS thickness overlaid on the Zn · Ph was approximately 2 mil. The total area of film that comes into contact with NaCl solution was 6.0×10^3 mm^2. A defect was made using a 1-mm diameter drill bit. After exposure, specimens were removed from the cell and allowed to dry. The PPS coating was removed by cutting, revealing a delaminated region that appeared as a light gray area adjacent to the defect.

To evaluate the durability of the PPS/substrate interfacial bond, the lap-shear tensile strength of substrate-to-substrate PPS adhesive specimens was determined after exposure to H_2SO_4 solution (pH $\approx$ 3) containing 0.1 M NaCl for up to 8 days at 80°C. The lap-shear tensile strength was estimated in accordance with the modified ASTM Method D-1002. Before overlapping the substrate strips, (50 mm long and 15 mm wide), the 10 × 15 mm lap area was coated with PPS adhesive. The thickness of the overlapped PPS film ranged from 1–3 mil. The bond strength of the lap-shear specimens is the maximum load at failure divided by the total bonding area of 150 mm^2.

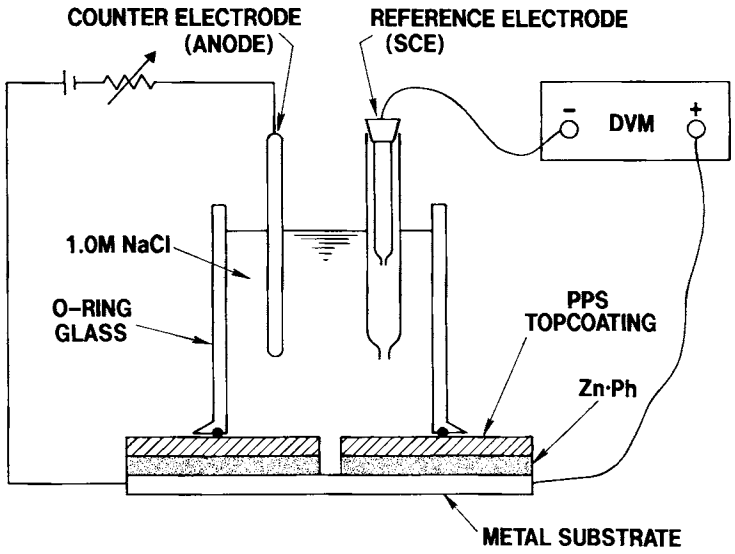

Figure 1 Schematic diagram of cathodic delamination test.

RESULTS AND DISCUSSION

Cathodic Delamination

As discussed in the introduction, it is very important to identify the species of phase present in the anhydrous Zn · Ph layers that greatly influence the vulnerability to alkali attack. The degree of alkali dissolution of the α-$Zn_3(PO_4)_2$ phase was considerably lower than that of the γ-phase. To ascertain whether the dehydration phase of Zn · Ph derived from this zinc phosphate solution is α-phase, the Zn · Ph crystal layers were scraped from the steel surfaces before and after thermal dehydration at 350°C in the air and then ground to a size of 325 mesh (0.044 mm) for X-ray powder diffraction (XRD).

Figure 2 illustrates two XRD tracings; the original Zn · Ph, denoted as sample a, and the anhydrous Zn · Ph (sample b) prepared by heating the original sample at 350°C. Two hydrous crystal phases were distinguishable in the original Zn · Ph layers, namely, zinc orthophosphate dihydrate [$Zn_3(PO_4)_2 \cdot 2H_2O$] present as the major component and hopeite [$Zn_3(PO_4)_2 \cdot 4H_2O$] as the minor one. The predominating phase of the anhydrous samples is identical to α-$Zn_3(PO_4)_2$, and γ-$Zn_3(PO_4)_2$ is present as a secondary phase. This result was in agreement with that obtained in our previous investigation,[5] that is, $Zn_3(PO_4)_2 \cdot 2H_2O$ was converted into the α-$Zn_3(PO_4)_2$ phase during dehydration and the $Zn_3(PO_4) \cdot 4H_2O \rightarrow \gamma$-$Zn_3(PO_4)_2$ phase transition is favored. Hence, we can predict that the anhydrous Zn · Ph layers prepared in this study will have a minimum rate of alkali dissolution.

Figure 3 shows the delaminated area of PPS film

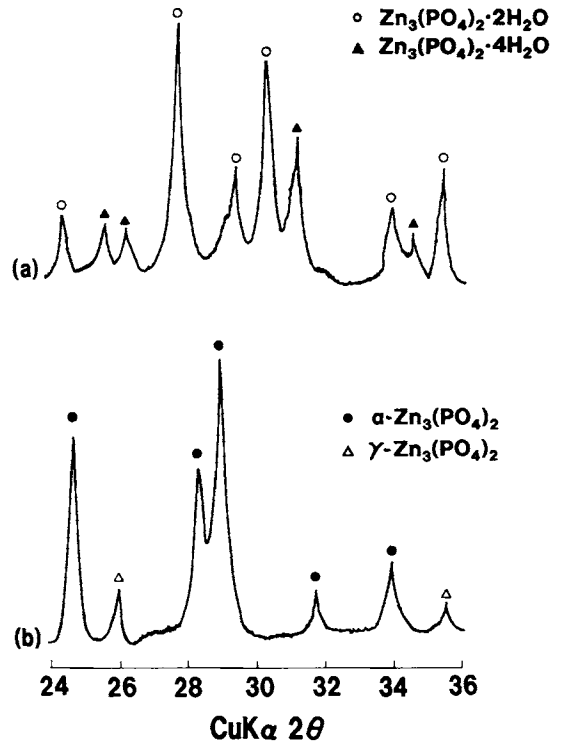

Figure 2 XRD tracings for (a) the original Zn · Ph samples and (b) the 350°C dehydrated Zn · Ph samples.

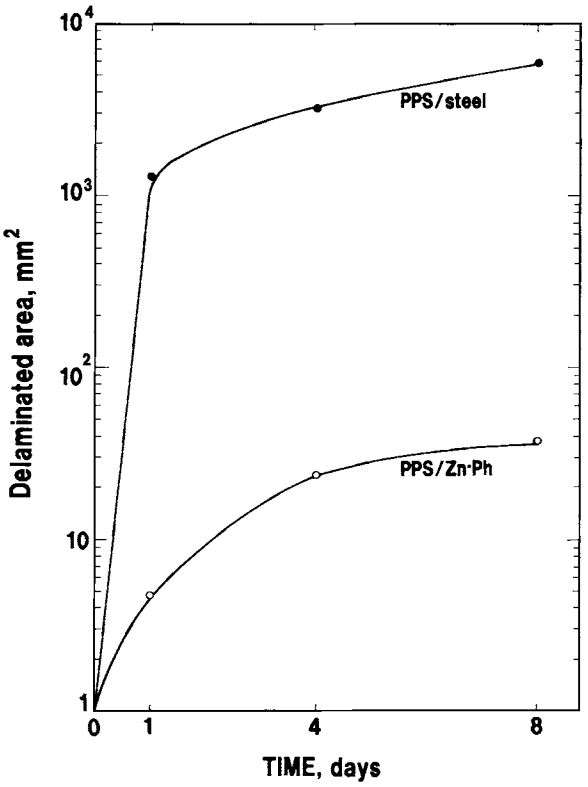

Figure 3 Cathodic delamination of PPS film from steel and Zn · Ph-deposited steel substrates in 1.0*M* NaCl.

from the substrates after up to 8 days of cathodic testing. For PPS/steel joint systems in the absence of Zn · Ph, the resulting curve indicates that there is a significantly large area of delamination of PPS after only 1 day's exposure. Further exposure up to 8 days resulted in an extensive delamination of $\approx 6 \times 10^3$ mm^2. The rate of delamination of this PPS/steel system was considerably reduced when Zn · Ph was deposited onto the steel surfaces. The value of $\approx 4 \times 10$ mm^2 for the PPS/Zn · Ph system obtained after 8 days was $\approx 10^2$ times lower than that of the PPS/steel system after the same exposure. Why such a high rate of delamination occurs at the critical interfacial zones of the PPS/steel systems is of particular interest. To gain this information, we explored by XPS both cathodically failed PPS and steel interfaces for 8-day-exposed PPS/steel systems. For purposes of comparison, both failure sides for the unexposed control systems were investigated. The control samples were prepared by pulling the PPS films from the steel and Zn · Ph substrate surfaces at sites of tension failure. Table I summarizes the chemical compositions of the cross-section samples before and after the cathodic experiments. For the controls, the interface chemistry of the PPS side removed from the steel substrate consists of 3.5% S, 42.1% C, 44.0% O, and 10.4% Fe. The S element refers to S originating from the fundamental formula, $[\text{-}\langle\bigcirc\rangle\text{-S-}]_n$, of PPS. The C belongs both to carbons in the PPS and in the contaminants. As reported in our previous paper,[1] the Fe and O elements remaining on the PPS side are associated with the interfacial reaction products formed by interaction between the PPS coating and Fe_2O_3 existing at the outermost surface site of steels. No S atom was found on the failed steel sides. Thus, it appears that the locus of failure occurs through the reaction product layers close to PPS. A striking difference from the control was observed in the cathodically delaminated samples. The differences are as follows: (1) A large amount of Fe and O was removed from the interfacial PPS sides, while the concentrations of S and C were markedly increased; (2) a small amount of S remained on the steel sides; and (3) a certain amount of Na from the NaCl electrolyte was detected on both the delaminated PPS and steel sides. There was no evidence for the presence of the Cl atom. The first two results show that the cathodic reaction, $H_2O + \frac{1}{2}O_2 + 2e^- = 2OH^-$, occurring at the defect in the PPS film leads to the elimination of Fe-related reaction products. Since the ionic reaction between the OH^- ions generated by cathodic reaction and the Na^+ ions dissociated from NaCl electrolyte yields a high concentration of NaOH in the area of the defect,[8] it is reasonable to assume that creation of such an alkali environment at the interfacial regions cause NaOH-catalyzed hydrolysis of the interfacial reaction products. Thus, as a result of difference 3, the detection of Na atom at the delaminated interfaces could be due to the penetration of the NaOH solution through the interfacial layers.

To support this hypothesis, we inspected the high-resolution S_{2p} core-level spectra of the PPS and steel

Table I Chemical Composition of Both Interfacial Failure Sides Before and After Cathodic Delamination Tests for PPS/Steel Joint Systems

Cathodic Test	Failed Side	Atomic Concentration, %					
		S	C	O	Mn	Fe	Na
Before	PPS	3.5	42.1	44.0	—	10.4	—
Before	Steel	—	31.3	55.5	0.7	12.6	—
After	PPS	10.7	80.9	6.1	—	1.5	0.8
After	Steel	1.3	23.3	59.6	1.3	13.3	1.2

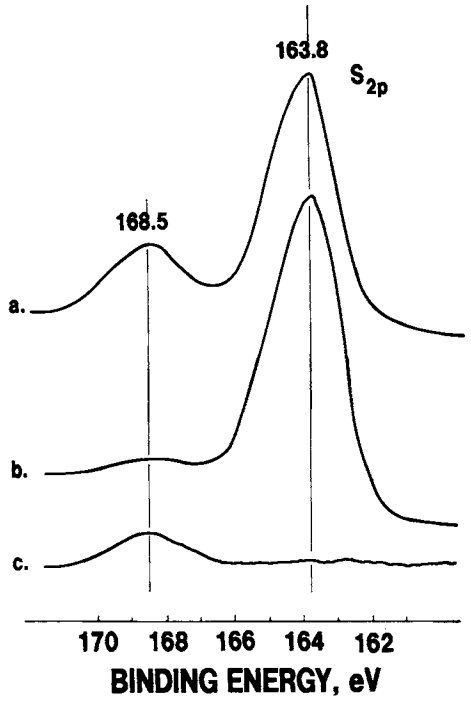

Figure 4 S_{2p} core level spectra for (a) the PPS side removed from the steel before cathodic delamination tests and (b) the delaminated PPS and (c) steel sides after cathodic tests.

interfacial sides of the specimens before and after cathodic tests (Fig. 4). The S_{2p} region for the PPS interface of the control samples reveals two major components at 163.8 and 168.5 eV. The former peak, the principal component, is attributable to the S in the PPS, while the latter reflects the S in the ferrous sulphate ($FeSO_4$) formed by the interfacial gas–solid reaction between Fe_2O_3 and SO_2 and SO_3 gases emitted from PPS in air at a high temperature.[1] By comparison with the control, the remarkable attenuation of peak intensity at 168.5 eV originating from the Fe in the $FeSO_4$ reaction product can be observed on spectrum (b) of the cathodically delaminated PPS side. In the spectrum (c) of the delaminated steel side, the presence of weak line at 168.5 eV verifies that a small amount of intermediate $FeSO_4$ adhering to the steel remains at the interfacial steel side, while there are no signals for the peaks of 163.8 eV corresponding to the PPS. Therefore, the major reason for the more extreme cathodic delamination at PPS/steel interfaces was the NaOH-catalyzed hydrolysis of $FeSO_4$ adjacent to the steel surfaces.

Table II gives the elemental compositions for both interfacial failure sides in the PPS/Zn · Ph joint systems before and after cathodic tests for 8 days. The interfacial PPS surface of control samples had a composition closely resembling that of the Zn · Ph interface except that there was no S element. The detection of a certain amount of P, Fe, and Zn on the PPS interface demonstrated that these elements migrate from the Zn · Ph-covered steel substrate to the coating sides during the failure of the bond. These results show that there is a good interfacial bond between PPS and Zn · Ph. Hence, failure must occur through the Zn · Ph layer. In other words, the PPS-to-Zn · Ph bond strength is much greater than that of Zn · Ph itself. A dramatic change in composition can be seen on both of the cathodically delaminated areas of the interfacial PPS and Zn · Ph sides, namely, a remarkable amount of P, O, Fe, and Zn has vanished from the delaminated areas, while additional amounts of Na atom have been incorporated into the interfaces. The data also suggested that the rate of elimination of Fe atom is much higher than that of any other elements. The removal of P and Zn may be mainly due to the dissolution of Zn · Ph layers caused by the attack of alkali solution generated by the oxygen reduction reaction ($H_2O + \frac{1}{2}O_2 + 2e^- = 2OH^-$) at the site of the defect. Since the evolved OH^- ions ionically react with Na^+ dissociated from NaCl, the incorporation of Na can be directly related to the penetration of NaOH yielded by this charge balance into the failure zones. Such alkali dissolution of the Zn · Ph layers is reflected in the increase in concentration of S and C atoms in the PPS. But an important question still remains to be answered. Why is the rate of elimination of Fe-related compounds considerably higher than that of the Zn · Ph? To answer this question, we inspected the high-resolution P_{2p}, $Zn_{2p3/2}$, $Fe_{2p3/2}$, and S_{2p} spectra of the cathodically delaminated PPS side and the PPS failure surface that was made by pulling the PPS film from the Zn · Ph before the

Table II Chemical Composition of Both Interfacial Failure Sides Before and After Cathodic Delamination Tests for PPS/Zn · Ph Joint Systems

Cathodic Test	Failed Side	Atomic Concentration, %						
		P	S	C	O	Fe	Zn	Na
Before	PPS	8.5	2.5	32.0	47.1	6.1	3.8	—
Before	Zn · Ph	5.3	—	35.9	47.7	8.1	3.0	—
After	PPS	3.4	4.1	56.2	26.9	0.4	2.1	6.9
After	Zn · Ph	2.1	1.5	56.8	31.5	0.9	2.5	4.7

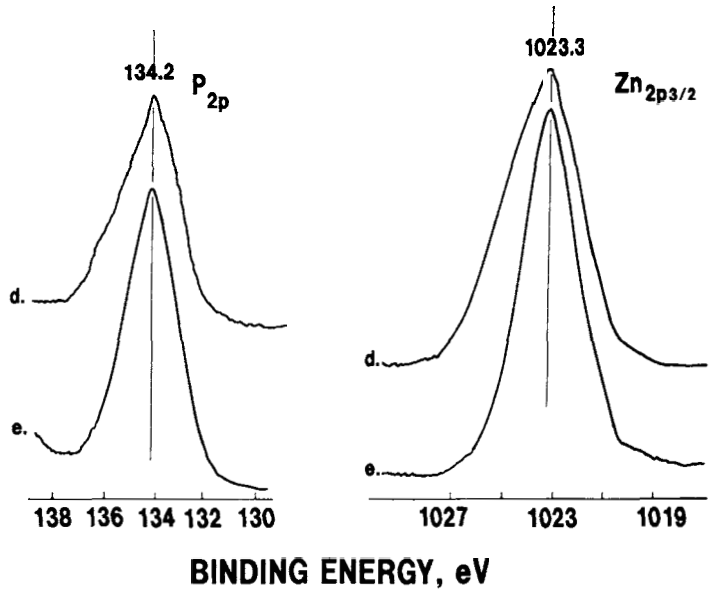

Figure 5 P_{2p} and $Zn_{2p3/2}$ regions for (b) the interfacial PPS sides before cathodic test and (e) at the cathodically delaminated PPS interface.

cathodic tests. Figure 5 illustrates the resultant P_{2p} and $Zn_{2p3/2}$ regions of these samples. The control sample (before cathodic tests), denoted as d, had a main line at 134.2 eV for P_{2p} and at 1023.3 eV for $Zn_{2p3/2}$ spectra, reflecting the P and Zn atoms in Zn · Ph.[9] Peak features and intensity similar to those of the control was observed in both the P_{2p} and the $Zn_{2p3/2}$ region for the sample (e) after cathodic tests. In the $Fe_{2p3/2}$ region (Fig. 6), the control sample (d) displays a strong signal emerging at the BE position of 710.7 eV, corresponding to the formation of ferric oxide (Fe_2O_3).[10] Since the electrochemical reaction between the steel and Zn · Ph solution at an early stage of Zn · Ph precipitation leads to the liberation of the free Fe ions from the steel surface,[11] it is not surprising that Fe_2O_3 forms by the oxidation of free Fe present in the Zn · Ph layers during the $Zn_3(PO_4)_2 \cdot 2H_2O \rightarrow \alpha\text{-}Zn_3(PO_4)_2$ phase conversion

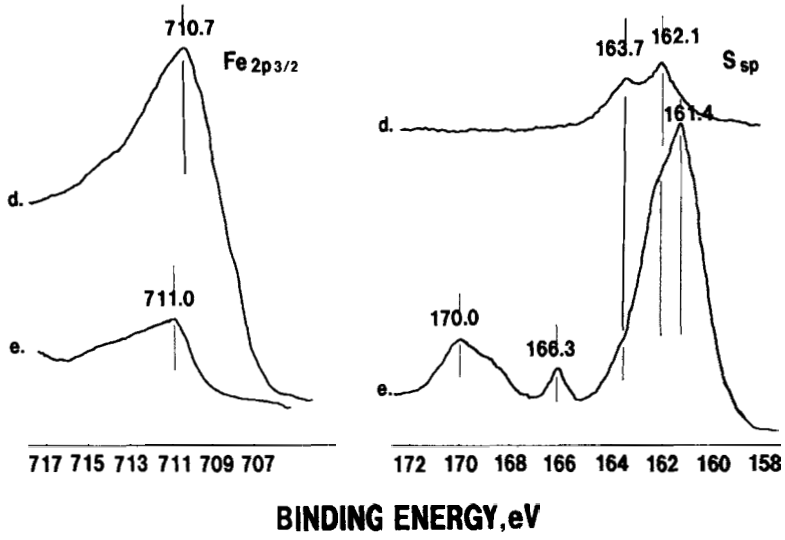

Figure 6 $Fe_{2p3/2}$ and S_{2p} regions for (d) the interfacial PPS side before cathodic test and (e) at the cathodically delaminated PPS interface.

in air at 350°C before the PPS coating is deposited. In fact, we observed color changes in Zn · Ph coating, from a dark gray at 100°C to a light brown at 350°C. A striking decay in the $Fe_{2p3/2}$ signal intensity was observed from the cathodically delaminated PPS interface (e) (the reason will be discussed later). The S_{2p} region (Fig. 6) for the control (d) reveals two resolvable components at 163.7 and 162.1 eV. The former peak is attributable to the S in the PPS, and the latter belongs to the S in the FeS.[12] This information seems to suggest that the SO_2 gas emitted from the PPS in the vicinity of Zn · Ph layer preferentially reacts with Fe_2O_3 in the Zn · Ph layers, rather than the α- and γ-$Zn_3(PO_4)_2$ phases. To confirm that SO_2 was taken up by Fe_2O_3, anhydrous Zn · Ph coatings were exposed in SO_2 gases at 350°C (flow rate $\approx$ 200 cc/min) for up to 120 min. The chemical compositions of the exposed coating surfaces were investigated by XPS, and then the internally generated P_{2p}, S_{2p}, Fe_{2p}, and $Zn_{2p3/2}$ peak areas were used to calculate the atomic percent ratios. Figure 7 shows the variation in P/Zn, S/Zn, and Fe/Zn ratios as a function of exposure times. The data indicate that the value of the S/Zn ratio increases with longer exposure time, while the Fe/Zn ratio value monotonously decreases as a function of time. In contrast, the P/Zn ratio does not express any changes in value for the exposure periods up to 120 min. Thus, these data strongly support the idea that SO_2 is taken up by the Fe_2O_3 present in the Zn · Ph layers.

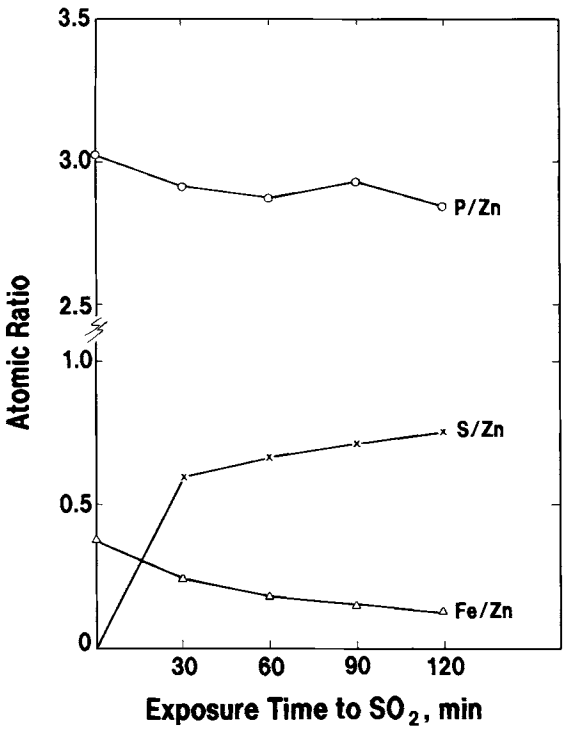

Figure 7 Changes in P/Zn, S/Zn, and Fe/Zn atomic ratios as a function of exposure time to SO_2.

Returning to the S_{2p} spectrum in Figure 6, the drastic changes in spectral features occur as the cathodic reaction is initiated at the defect. In particular, the S_{2p} signal at the cathodically delaminated PPS side (e) was characterized by the appearance of three new peaks, the most intense peak being at 161.4 eV, with two prominent lines at 166.3 and 170.0 eV. Considering that there is little residual Fe atom at the delaminated PPS side, these new lines do not reflect the formation of Fe-related sulfur compounds. However, since a large amount of Na remains on the delaminated PPS interface, these lines possibly could be assigned to the Na-related sulfur compounds derived from the cathodic reaction. Assuming that these predicted assignments are correct, other authors[13] suggested that the predominating line at 161.4 eV is due to the S in the sodium sulphide (Na_2S) as the major by-product of the cathodic reaction; the other lines at 166.3 and 170.0 eV were ascribed to the sodium sulphite (Na_2SO_3) and sulphate (Na_2SO_4), respectively. The striking decay of $Fe_{2p3/2}$ signal [Fig. 6(e)] at the cathodically delaminated PPS side can be interpreted as follows: The Fe_2O_3 in Zn · Ph layers favorably reacts with PPS to form FeS, which is one of several S-related iron reaction compounds. However, it was very difficult to distinguish the photoelectron line of FeS from the Fe_2O_3 line in the $Fe_{2p3/2}$ region because the signal originating from Fe in FeS emerges at only $\approx$ 0.3 eV lower BE position than that of Fe_2O_3.[14] Nevertheless, the decay of $Fe_{2p3/2}$ signal was implicated in the loss of a great deal of FeS caused by NaOH-catalyzed hydrolysis.

Using SEM and EDX, we also investigated the morphology and the elemental distribution of cathodically failed Zn · Ph side (Fig. 8). As seen in the bottom left photograph of Figure 8, SEM topography reveals the existence of two distinctive areas: site A represents an area approximately 1000 μm in diameter surrounding the defect, while site B is at the edge of the delaminated PPS. The C area in the top photograph, an enlargement of site A, discloses the presence of the PPS adhering locally to the substrate. As is evident from the EDX elemental data from this region, a small part of the PPS film remaining on the substrate contains not only the S atom but also has other elements such as Na, Fe,

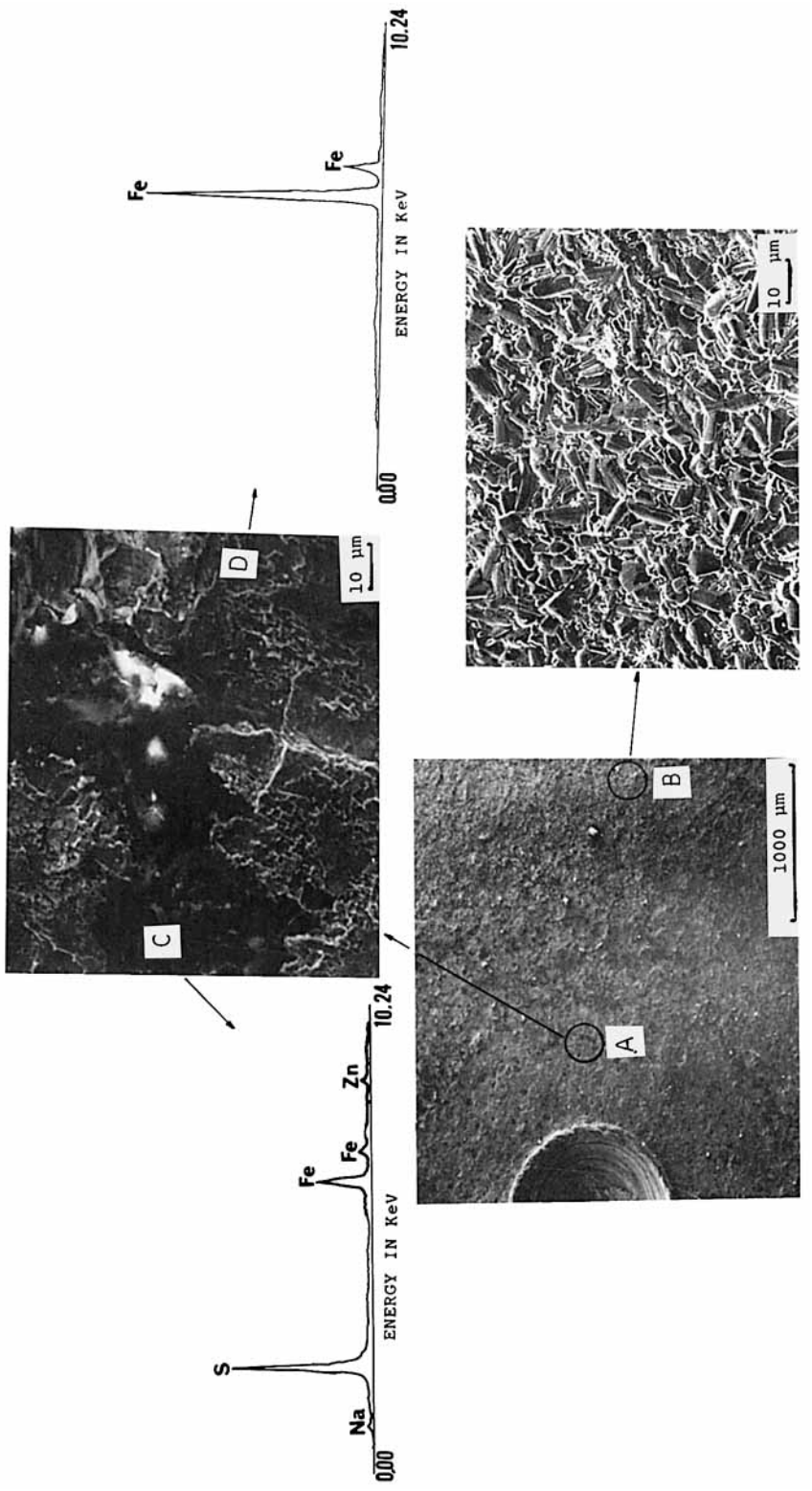

Figure 8 SEM microprobe and EDX spectra of the cathodically delaminated area (A) near a defect and (B) at the delaminated front of anhydrous Zn · Ph coating after PPS was removed from the PPS/Zn · Ph joint.

and Zn. The EDX spectrum of area D in the same photograph, representing the presence of the Fe atom alone, relates to the steel substrate. These findings strongly suggested that almost all the crystalline conversion coating surrounding the defect was dissolved in the NaOH solution resulting from the cathodic reaction occurring beneath the PPS film. The right-bottom SEM microstructure (an enlargement of site B) is an image of the morphology of a normal Zn · Ph crystal coating, which has not been attacked by NaOH.

A certain amount of p(AA) polyelectrolyte incorporated during crystal growth into the zinc phosphate solution is present at the outermost surface sites of Zn · Ph layers.[15] Thus, we should consider whether there is an interaction between p(AA) and PPS. In an attempt to obtain this information, samples were prepared in the following way: First, the steel plate was dipped for 5 min into the 1.0% p(AA) aqueous solution, and then dried in an oven at 350°C for 1 h to transform the p(AA) macromolecule from the poly(acid), having COOH pendent groups, to the poly(acid)anhydride having

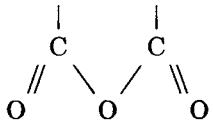

and COOH groups.[16] A PPS slurry was then deposited on the poly(acid)anhydride macromolecule film surfaces, followed by curing in air at 350°C. Finally, the PPS site removed from the poly(acid)-anhydride-primed steel was inspected by XPS. Figure 9 shows the XPS spectra for the C_{1s} region of the bulk PPS film (f) and for the interfacial PPS site (g). For the bulk PPS, the single peak at 285.0 eV reveals the aromatic hydrocarbon in PPS. By comparison with the symmetry of the curve of bulk PPS, the shape of the peak of the samples from the interfacial PPS site has an asymmetric tailing toward the high BE sides. This tail, which separates from the primary peak of aromatic hydrocarbon at 285.0 eV, reveals the presence of at least two resolvable peaks. Based upon published data,[17] the assignments of the lines at 288.1 and 289.3 eV are due to the carbon in the carboxyl (C=O) group and the carboxylic acid (COOH) group, respectively, thereby suggesting that bond failure occurs through the mixing layers of PPS and poly(acid)anhydride. Although there is no evidence about the interfacial bond structure and the chemical or physical interactions, it appears that the poly(acid)anhydride macromolecule has a strong affinity for PPS. On the other hand, the rough surface structure of crystalline Zn · Ph was one factor contributing to the increased mechanical interlocking forces associated with the mechanical anchoring of the PPS polymer, resulting from the penetration of the melted polymer into the open-surface microstructure and microfissures of Zn · Ph layers. Consequently, the combination of such chemical and physical bond structures plays a major role in the good adhesion performance at PPS-to-Zn · Ph joints.

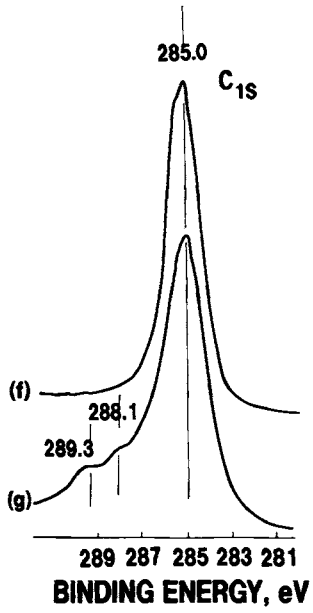

Figure 9 C_{1s} spectra for (f) bulk PPS and (g) PPS interface removed from poly(acid)anhydride-primed steel.

Durability of Adhesive Bond

As discussed, the cathodic delamination of PPS film from a zinc-phosphated steel was due primarily to the alkali dissolution of Zn · Ph and FeS underneath the PPS coatings. We investigated the durability of the steel/ and Zn · Ph/PPS adhesive bonds after exposure at 80°C to H_2SO_4 solution (pH $\approx$ 3) containing 0.1 *M* NaCl. All edges on the PPS adhesive/adhered joints were unprotected to evaluate the susceptibility of the interfacial bonding to the hot acid. Figure 10 shows the changes in the value of lap-shear bond strength as a function of exposure time; each value in the figure represents the average of three measurements. For the unexposed control specimens, the bond strength of the PPS/Zn · Ph joint was much higher than that of the PPS/steel joint. The deposition of Zn · Ph layer on the steel surface appears to provide a strong adhesive bonding of PPS/steel joints. The data for the PPS/Zn · Ph specimens indicated that a reduction in strength gradually occurs during exposures of up to 4 days; beyond this, there is very little reduction in strength.

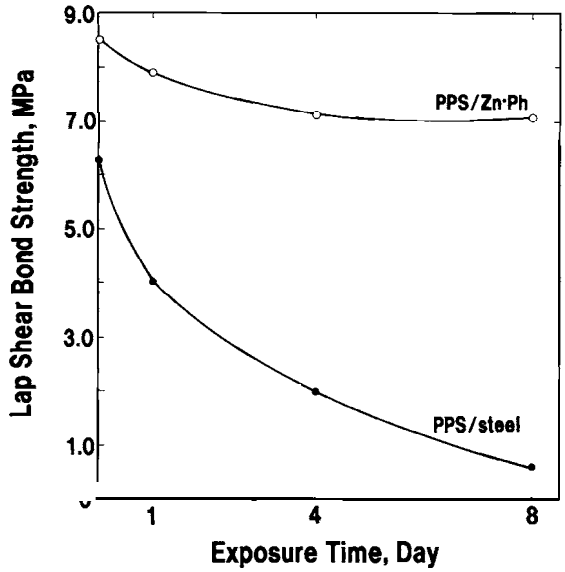

Figure 10 Lap-shear bond strength vs. exposure time to 80°C H_2SO_4 solution.

This fact is reflected in the considerable durability of the PPS/Zn · Ph joint in hot-acid environments. The SEM image (not shown) of peeled PPS interface for the 8-day-exposed specimens showed the presence of a large amount of Zn · Ph, suggesting that the mode of delamination can be defined as cohesive failure that occurs through the Zn · Ph layer. In contrast, the strength of the PPS/steel specimens after exposure for 8 days dropped dramatically to a value of 0.6 MPa, a reduction of $\approx$ 89%. There was a partial separation of the PPS film from the steel surface, thereby implying that the bond durability of PPS/steel joints is very poor.

To elucidate the failure mode of acid-damaged PPS/steel joints, the PPS-coated steel specimens were exposed for 8 days at 80°C in H_2SO_4 solution (pH $\approx$ 3) containing 0.1*M* NaCl. After exposure, the chemical composition of the separated PPS and steel interfaces was inspected by XPS; the quantitative data are given in Table III. Compared with the control specimens, the interfaces of the exposed specimens were characterized by representing the migration of S atom from the PPS to the steel sides and the interfacial diffusion of Cl. There was no signal for Na from the formation of Na-related sulfur reaction compounds, which are induced by the diffusion of Na ions into the interfacial boundary zones. Nevertheless, the locus of failure appears to occur through the S-incorporated reaction product layers as means of the adhesive failure at the interface.

Table III Atomic Concentrations of Failed PPS and Steel Sides Before and After Exposure for 8 Days to 80°C H_2SO_4 Solution

Exposure to H_2SO_4	Failed Side	Atomic Concentration, %					
		S	C	O	Mn	Fe	Cl
Before	PPS	3.5	42.1	44.0	—	10.4	—
Before	Steel	—	31.3	55.5	0.7	12.6	—
After	PPS	6.7	20.9	63.0	—	7.8	1.6
After	Steel	3.1	18.4	65.0	—	11.2	2.3

To identify the reaction product that causes the bond failure in hot acid, we inspected S_{2p} core-level spectra for both the separated PPS and the steel sides (Fig. 11). The S_{2p} region for both sides showed the emergence of a single peak at the position of 169.0 eV, which corresponds to a shift of 0.5 eV to the higher BE site than that of $FeSO_4$, formed by interaction between PPS and the steel [see Fig. 4(a)] before exposure. A shift of 0.5 eV is reasonable to distinguish the formation of ferric sulphate $[Fe_2SO_4)_3]$,[13] which may be generated by H_2SO_4-catalyzed oxidation of $FeSO_4$. Thus, the cause for the bond failure of PPS/steel joints after exposure to hot-acid solution was the interfacial $FeSO_4 \rightarrow Fe_2(SO_4)_3$ phase transition.

CONCLUSIONS

When high-temperature performance PPS polymer coatings were directly applied to cold-rolled steel surfaces, the chemical reaction at 350°C between the Fe_2O_3 at the outermost surfaces of the steel and

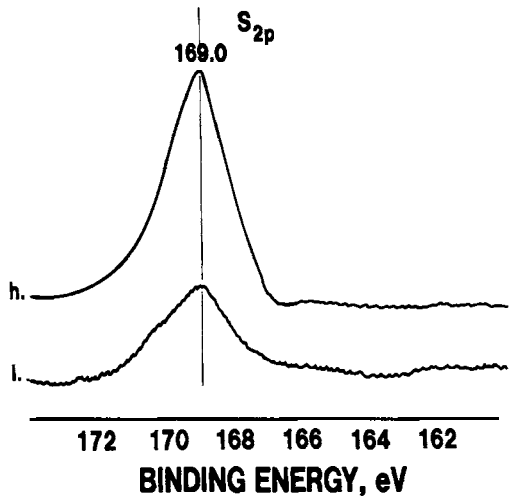

Figure 11 S_{2p} region for (h) PPS and (i) steel interfaces separated by the attack of hot-acid solution on the PPS/steel joint.

the PPS in air led to the formation of $FeSO_4$ at the critical interfacial zones. Although the intermediate $FeSO_4$ layers, as interfacial reaction products, play an important role in developing bond strength at the PPS/steel joint, the alkali-catalyzed hydrolysis of $FeSO_4$ caused by the cathodic reaction, $H_2O + \frac{1}{2}O_2 + 2e^- = 2OH^-$, at any defects in the coating film caused catastrophic cathodic delamination of the PPS film from the steel. Therefore, to avoid the direct contact of PPS with steel, a p(AA)-modified Zn · Ph conversion coating was deposited on the steel surfaces. Before applying the PPS, the $Zn_3(PO_4)_2 \cdot 2H_2O$ as major phase of the Zn · Ph layers was converted into an α-$Zn_3(PO_4)_3$ phase by thermal dehydration at 350°C. This thermal treatment also promoted the transformation of the poly(acid) structure within the p(AA) into the poly(acid)anhydride and the oxidation of free Fe atoms dissociated from the steel surfaces during the precipitation of the crystalline Zn · Ph coating. We found that SO_2 emitted from the PPS at the PPS-to-Zn · Ph boundary regions preferentially reacts with the oxidized Fe compounds rather than with Zn and P atoms in the Zn · Ph crystals. Such a gas–solid interaction between SO_2 and the oxidized Fe compound at 350°C caused the formation of an FeS reaction product. In addition, two different interactions were recognized: One was the polymer-to-polymer reaction between the PPS and the poly(acid)anhydride existing at the outer surface of the Zn · Ph layers; the other was the mechanical interlocking associated with the mechanical anchoring of the PPS polymer, which resulted from the penetration of the melted polymer into the open surface microstructure of the Zn · Ph layers. These physicochemical factors, contributing to the development of adhesion force at the PPS/Zn · Ph interfaces, were essentially responsible for the high lap-shear bond strength on the phosphated metal-to-phosphated metal PPS specimens.

Once a cathodic reaction occurs at a defect in the PPS/Zn · Ph system, the action of NaOH derived from the cathodic reaction results in the dissolution and hydrolysis of the anhydrous Zn · Ph and FeS interaction product. Such an alkali-induced dissociation resulted in the formation of the Na-related sulfur compounds, such as Na-sulphide, Na-sulphite, and Na-sulphate. However, the rate of cathodic delamination of PPS for the PPS/Zn · Ph system was considerably lower than that for the PPS/steel system.

The adhesive bonds of the PPS/Zn · Ph systems displayed an outstanding bond durability against attack by a hot H_2SO_4 solution containing NaCl. In contrast, the bonds of the PPS/steel systems failed after exposure for only 8 days to this hot-acid solution. The major reason for this failure was due to $FeSO_4 \rightarrow Fe_2(SO_4)_3$ phase transformation in the intermediate layers. The formation of $Fe_2(SO_4)_3$ may be deduced from the acid-catalyzed oxidation of the $FeSO_4$ reaction product formed at the PPS/steel interfaces.

This work was performed under the auspices of the U.S. Department of Energy under Contract No. DE-AC02-76CH00016 and supported by the U.S. Army Research Office Program MIPR-ARO-119-91 and the Physical Sciences Department of the Gas Research Institute under Contract No. 5090-260-1948.

REFERENCES

1. T. Sugama and N. R. Carciello, Int. *J. Adhesion Adhesives,* **11,** 97 (1991).
2. J. B. Sardisco and R. E. Pitls, *Corrosion,* **21,** 245 (1965).
3. C. Milton, *Corrosion,* **22,** 191 (1966).
4. A. L. Martin and R. R. Annand, *Corrosion,* **36,** 297 (1981).
5. T. Sugama and J. Pak, *Adv. Mater. Manuf. Proc.,* **6,** 227 (1991).
6. T. Sugama, L. E. Kukacka, N. Carciello, and J. B. Warren, *J. Mater. Sci.,* **26,** 1045 (1991).
7. M. P. Seah and W. A. Dench, *Surf. Interface Anal.,* **1,** 2 (1979).
8. H. Leidheiser Jr. and W. Wang, in *Corrosion Control By Organic Coatings,* H. Leidheiser, Jr. (ed.), NACE, Houston, TX, 1981, pp. 70–77.
9. T. Sugama, L. E. Kukacka, N. Carciello, and J. B. Warren, *J. Coat. Tech.,* **61,** 43 (1989).
10. N. S. McIntye and D. G. Zetaruk, *Anal. Chem.,* **49,** 1521 (1977).
11. T. Sugama, L. E. Kukacka, N. Carciello, and J. B. Warren, *J. Mater. Sci.,* **22,** 722 (1987).
12. H. Binder, *Z. Natürforsh,* **B28,** 255 (1973).
13. B. J. Lindberg, K. Hamrin, G. Johanson et al., *Phys. Scr.,* **1,** 277 (1970).
14. J. C. Carver, G. K. Schweitzer, and T. A. Carlson, *J. Chem. Phys.,* **57,** 973 (1972).
15. T. Sugama, L. E. Kukacka, N. Carciello, and J. B. Warren, *J. Mater. Sci.,* **23,** 101 (1988).
16. T. Sugama, L. E. Kukacka, C. R. Clayton, and H. C. Hua, *J. Adhes. Sci. Tech.,* **1,** 265 (1987).
17. D. Briggs and M. P. Seah, *Practical Surface Analysis by Auger and X-ray Photoelectron Spectroscopy,* John Wiley, New York, 1985, p. 385.

Received March 25, 1991
Accepted September 3, 1991